Experience Report of Potential Free Temperature Measurement with commercially available Pyrometers in gas insulated systems

Dipl.-Ing. Martin Hallas, Technical University of Darmstadt, Germany, martin.hallas@tu-darmstadt.de
Julian Moxter M.Sc., Technical University of Darmstadt, Germany, julian.moxter@tu-darmstadt.de
Prof. Dr.-Ing. Volker Hinrichsen, Technical University of Darmstadt, Germany, volker.hinrichsen@tu-darmstadt.de
Dipl.-Ing. Karsten Juhre, Siemens Energy, Berlin, Germany, karsten.juhre@siemens-energy.com
Dr.-Ing. Michael Tenzer, Siemens Energy, Erlangen, Germany, michael.tenzer@siemens-energy.com

Abstract

A potential free temperature measurement in gas insulated switchgear and lines (GIS/GIL) was investigated within an HVDC research project, because the temperature is of high importance during development and operation of HVDC equipment. Infrared spectrum measurement of the heated inner conductor by pyrometer sensors has emerged as the best technical solution for HVDC GIS/GIL. To optimize the infrared emission of the inner conductor, it was painted with black varnish. The sensor had to be adjusted to the infrared transmission of the pressurized insulating gas atmosphere. Experiences as well as methods to perform such a calibration are shown in the paper. A calibration by adjusting transmission and emission coefficients inside the sensor software did not succeeded, because the coefficients differed for variable sensor ambient temperatures. A successful calibration was possible by considering two major variables: the pyrometer output as well as the sensor ambient temperature. However, certain limits of the pyrometer measurement in GIS/GIL were observed as well. The EMC performance of the pyrometer was improved by an additional electronic unit, which protects the commercial electronics. Overall, the potential free temperature measurement could be performed during the long-term operation of the regarded HVDC GIL system. Typical temperature curves based on the calibrated pyrometer sensor are shown.

1 Introduction

A particular challenge in the design of HVDC stressed gas insulated equipment (GIS and GIL) is the accumulation of electrical charge carriers at the gas-insulator interfaces and in the bulk of the insulating material, which can cause locally increased electric field stresses [1]. During operation, a current flows through the high-voltage conductor, resulting in an inhomogeneous temperature distribution in the solid epoxy insulators and their environment. Since the electric field distribution under DC stress is mainly determined by the conductivities of the applied insulating media and as the conductivity of epoxy is strongly temperature dependent, the temperature distribution has thereby a major impact on the electric field distribution and on the overall dielectric performance of the insulation system. Since temperature has such a high impact, the question was raised during research on gas insulated HVDC equipment, how to monitor the temperature gradient along the insulation. For this purpose, the temperature of the inner conductor has to be measured while high voltage is applied. The possibility of potential free temperature measurement in a SF_6/N_2 gas insulated system was therefore investigated in the frame of a CIGRE prototype installation test on a ±550 kV DC GIL assembly at Technical University of Darmstadt [2]. Several options of potential-free temperature measurements of the inner conductor were discussed. Some of these are:

- Optical fibre sensors
- Battery powered temperature loggers
- Pyrometer sensors

Generally, optical sensors are a good choice in high voltage engineering. However, at HVDC the fibre would be stressed with the same temperature dependent charge effects as the rest of the insulation system. Since commercial fibres are not optimized to these effects, they might fail. Also, an embedding inside an insulator was not in favour since this would influence its field distribution and could cause failures as well. Besides, it would have been hard to realize.

In other projects good experiences were collected with battery powered data loggers [3], applied in gas insulated systems. Due to their compact design, they are often easy to implement, and the battery lifetime is often sufficient for many laboratory applications. However, in the project under consideration a long-term test was planned [2], potentially exceeding the expected battery lifetime during erection and testing. Changing the data logger during the test was no option as well since this would have modified the device under test [1]. Disadvantageously, no online temperature monitoring would have been possible and besides that, such electronic loggers also might get destroyed due to electromagnetic interferences (EMI) resulting from gas discharges after all. The measurement with a pyrometer placed at the enclosure was thus considered as the best choice to monitor the inner conductor temperature of the DC GIL.

https://www.vde-verlag.de/buecher/455978/etg-fb-169-vde-hochspannungstechnik-2022.html

1.1 Physics of Pyrometer Measurement

The pyrometer measurement is based on the principles of thermal radiation. A heated object emits electromagnetic radiation in the infrared spectrum (EMR). The spectral emission of a heated object is proportional to the fourth power of temperature [4]. Pyrometers make use of this correlation to determine the object temperature based on the measured radiation. Generally, the radiation balance in a physical body follows equation 1, where ε are the emission, φ the reflexion and τ the transmission factors. Each physical body hit by EMR has its own coefficients [4].

$$\varepsilon + \varphi + \tau = 1 \qquad (1)$$

The emission factor describes how much radiation is absorbed by a body. Ideal black bodies absorb all EMR, which results in $\varepsilon = 1$. The emissivity of conductor surfaces in the regarded gas insulated systems is difficult to determine, since ε not only depends on the used material, but also very sensitively on the surface condition. E.g. a blank, polished aluminum surface has a different ε compared to the same surface but with a more rough polishing, scratches or some grease due to touching [5]. Besides absorption of EMR some amount may also be reflected. This is described with the reflection factor φ. As ideal black bodies absorb all EMR, it results in $\varphi = 0$. Again, the treatment of the conductor surfaces in gas insulated systems strongly influence their reflection. Finally, the transmission factor τ describes how much of the EMR passes through an object. In many commercial applications this factor may be neglected, since no permeable materials like aluminum are measured, or pyrometers are often operated in ambient air with $\tau = 1$ in the chosen infrared range. Contrary to this, e.g. SF_6 absorbs certain amounts of infrared light. It has a low transmission factor in the wavelength range of (10…11) µm [6]. Transmission gets also important when the pyrometer measurement is performed through glasses or other permeable materials.

Since the setting of the factors ε, φ and τ is very specific, commercial pyrometers cannot be used "plug & play" in gas insulated systems. The sensors need to be adjusted to their specific environment, which is why a calibration of the sensor is required in order to apply them in the DC GIL research project (refer to section 2 and 3).

1.2 General Measurement Setup

The used measurement setup is shown in **Figure 1**. According to section 1.1 the overall EMR measurement is simplified for a black body with respect to its infrared emission and reflection. This means that the measured surface is desired to become a black body, so that reproducible surface conditions are set at all sensors and the pyrometer signal is maximized. Sticked-on foils or installation of other additional components were discussed but dropped, because all of them would have changed the outer shape of the inner conductor, influencing the electric field distribution of the DC GIL. Therefore, the aluminum

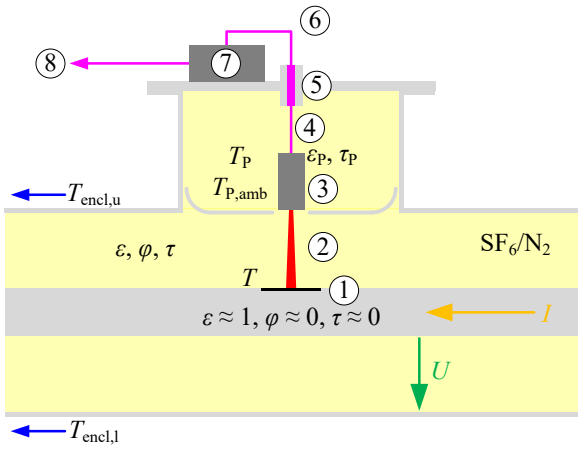

Figure 1 Pyrometer installation in a DC GIL; explanations in the text

surface was directly painted with a mat black varnish [11] of several micro-meters thickness (1). The varnish was chosen to be conductive in order to minimize the risk of surface charge effects at the painted surface under DC voltage stress, which might cause partial discharges during operation. In pre-investigations, optical and conventional electric partial discharge measurements were performed on painted objects under applied AC and DC voltage. Such measurements showed inconspicuous results, for which reason the varnish was rated to be uncritical for this application. The infrared emission (2) of the inner conductor at the temperature T passes the 40 % SF_6 / 60 % N_2 gas atmosphere. The atmosphere has unknown coefficients ε, φ and τ. The pyrometer sensor (3) [7] was installed inside the gas vessel in a flange of the earthed enclosure. The sensor was equipped with a surrounding electrode for electrical shielding purpose. The sensor type was chosen such that it is able to withstand the gas pressure and is applicable for the resulting distance between enclosure and conductor in terms of measurement range. Its measurement wavelength is in the range of (8...14) µm, for which reason the SF_6 damping in the range of (10…11) µm affects the sensor output. The sensor output is a temperature value T_P based on the measured infrared spectrum and the ambient temperature of the sensor $T_{P,amb}$. The radiation coefficients ε_P and τ_P could be adjusted at the sensor in order to adapt the sensor to different atmospheres and measurement surfaces. The sensor signal cable was cut into two parts (4) and (6) and connected via a gas tight low voltage bushing (5). The sensor cable was connected to its signal processing electronics (7) which had to be extended to improve the EMC performance of the system (refer to chapter 4). Finally, the electronics is connected to the control cubicle, which supplies the pyrometer with power and also hands over the sensor signal to the control unit. Additionally, the upper and lower enclosure temperatures $T_{encl,u}$ and $T_{encl,l}$ were measured with PT100 sensors.

2 Pre-investigations

First findings with the pyrometer measurement in gas insulated systems were gained in a built laboratory test arrangement (section 2.1). Two methods to set the sensor parameters for the SF_6/N_2 atmosphere were investigated (section 2.2 and 2.3). The overall findings gained with the commercial sensor in a gas insulated system are summarized in **Table 1**. Explanations are given below **Table 1**.

Table 1 Findings gained with pyrometers in gas insulated systems

(F1)	$T_P = f(T_{P,amb})$
(F2)	T_P~mV, $T_{P,amb}$~mV → high sensitivity to EMI
(F3)	Low EMC robustness against impulses of the electronics
(F4)	$\partial T_P/t \neq \partial T/t$ for small t
(F5)	$T_P \neq T$ if $T < T_{P,amb}$

(F1) The physics of thermal radiation is nearly independent from other parameters [8]. However, this is not the case for the used sensors [5][9]. Due to this, the pyrometer output T_P depends on its ambient temperature $T_{P,amb}$. Since the ambient temperature of a GIS/GIL enclosure may change due to sun radiation, current heating, etc., this needs to be considered.

(F2) The output signals of the pyrometer have a very low voltage magnitude in the 10 mV range. This makes the sensor output vulnerable to EMC of surrounded electrical devices.

(F3) Sensors as well as their signal processing electronics were observed to get destroyed just by regular high-voltage laboratory operation. E.g. damages occurred at sensors placed according to **Figure 2**, because of parallel breakdown voltage measurements in the same laboratory. The sensitive electronics inside the pyrometer is not optimized for high-voltage applications.

(F4) During operation of the sensor, it was observed that the sensor needs time to re-adjust the temperature in case of fast temperature changes [7]. This effect apparently became stronger when the sensor was placed in the gas insulated system.

(F5) A high measurement deviation between T_P and T was observed when the conductor temperature was lower than the enclosure temperature. For the pyrometer calibration these values should not be considered. However, this state is possible at ZL (zero load) condition of the gas insulated equipment (section 5.1).

2.1 Test Arrangement

The test arrangement was integrated in a large gas vessel (refer **Figure 2**). The pyrometer was installed similar to **Figure 1** at the earthed enclosure. To take "finding 1" into account, electrical heaters were placed near to the sensor. The temperature $T_{P,amb}$ could thereby be adjusted in the range of (20...50) °C. The heated conductor was modelled with an electrically heated and painted shell placed in the same distance to the conductor than in the later DC GIL test arrangement. Several thermocouples were placed at the

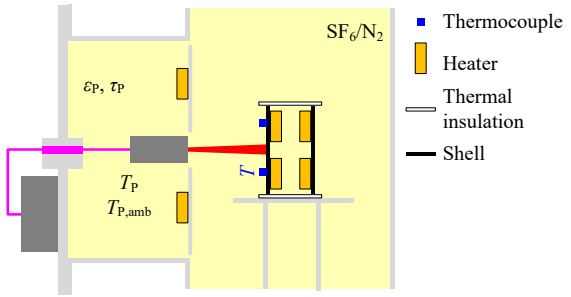

Figure 2 Test arrangement during pre-investigations

shell to measure the temperature T. The thermocouples were placed in drillings inside the shell filled with thermal paste, so that an optimal thermal contact was given. The conductor temperature was in the range of (20...90) °C. All electrical connections were made through gas tight electrical bushings. However, EMI at the sensor output ("finding 2") could not be avoided at this installation. Therefore, all heating devices had to be switched off before conducting a measurement. The overall arrangement and measurement uncertainty were checked by comparing T_P and T at a test arrangement in atmospheric air. Under these conditions $T_P = T$ had to be fulfilled. The measurement showed a good agreement of T_P and T in atmospheric air, which confirmed the test arrangement.

2.2 Adjustment of ε_P and τ_P

Generally, a correct adjustment of the pyrometer parameters ε_P and τ_P should be sufficient to use the sensor. Based on the values of T and $T_{P,amb}$ a measurement error below 2.5 K could only be achieved by setting the parameters to $\varepsilon_P = 0.95$ and $0.39 < \tau_P < 0.5$. An example for this observation is shown in **Figure 3**. For a constant average shell temperature $T \approx 89$ °C the ambient temperature $T_{P,amb}$ was increased. **Figure 3** shows that τ_P needs to be adjusted in order to stay below 2.5 K measurement error.

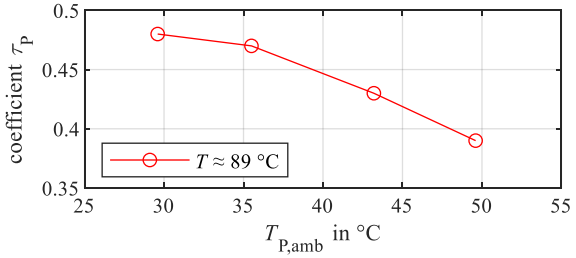

Figure 3 Adjusted pyrometer coefficient τ_P at different ambient temperatures, in order to keep the measurement error below 2.5 K

It had to be concluded, that the used sensor [7] cannot be applied in the gas insulated system by setting ε_P and τ_P to constant values, so that in the end certain pragmatic approaches had to be chosen.

2.3 $T = f(T_P, T_{P,amb})$

As a second approach the shell temperature T was defined as a function of the sensor output T_P at its standard coefficients $\varepsilon_P = 0.95$ and $\tau_P = 1$ and the sensor ambient temperature $T_{P,amb}$. In the pre-investigations a linear

behaviour was observed. **Figure 4** shows the linear relation between T_P and T for two fixed ambient temperatures $T_\mathrm{P,amb}$.

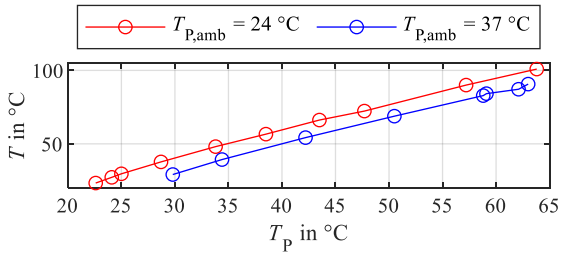

Figure 4 Linear relation between T_P and T for two ambient temperatures $T_\mathrm{P,amb}$

The linearity between T and T_P is nearly constant for different ambient temperatures $T_\mathrm{P,amb}$. Therefore, equation (2) can be generally stated.

$$T = f\left(T_\mathrm{P}, T_\mathrm{P,amb}\right) \tag{2}$$

2.4 Conclusions from the Pre-investigations

Based on the collected data of the pre-investigations a first approach in terms of measurement setup and data evaluation could be derived, as given in section 2.3 and equation (2). The on-site calibration (section 3) has shown that some measurements within the pre-investigations were inconsistent, for which reason these measurements are not presented in section 2. Therefore, a first formula derived from the pre-investigations and based on equation (2) also resulted in high measurement errors. The inconsistencies between pre-investigation and on-site calibration may result from the switch-off of all heating devices before measurement. This measure in combination with ”finding 4” listed in **Table 1** may have made the pre-investigation measurement vulnerable to measurement uncertainties.

Using a laboratory arrangement to calibrate a pyrometer sensor seems still to be feasible in principle. However, the findings listed in **Table 1** should be considered. The data logging needs to be taken very slowly to ensure correct re-adjustment of the sensor electronics to the new values. The EMC performance of the sensor should be increased (see section 4), so that calibration values can be logged, while all heating elements are switched on. It is recommended to start a sensor calibration in an enclosure filled with air at atmospheric pressure, to exclude all external influences as listed in **Table 1**, before starting the measurement in pressurized insulating gas.

3 On-Site Calibration

The pyrometer calibration in the real size DC GIL was planned for the end of the long-term test. At this moment, all required tools and test generators, like the gas handling equipment and the current source [10], were at site and fully installed. By use of the method presented in section 2.3, the collected sensor data and ambient temperature during the long-term test were used to calculate the temperature of the inner conductor based on the on-site calibration results.

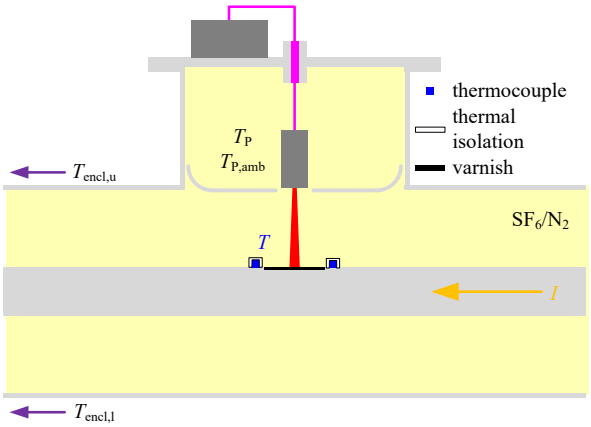

Figure 5 Test arrangement during on-site calibration

3.1 Test Arrangement

The test arrangement was according to **Figure 5**. In parallel to the pyrometer measurement, the temperature at the inner conductor of the DC GIL was measured with temporary installed thermocouples. These were embedded in thermal isolation in direction to the gas in order to ensure a measurement of the conductor temperature only. The overall arrangement was optimized compared to the pre-investigations by implementing all EMC countermeasures shown in section 4. This avoided errors due to EMI/EMC (“finding 2 and 3” of **Table 1)**. The heating of the conductor was performed with a DC current source of the test bay [10]. Compared to the pre-investigations, the overall heating and cooling of the arrangement took much longer transition times because of the higher thermal constants of the DC GIL arrangement. This avoided errors due to “finding 4” in **Table 1** and was thereby advantageous for the on-site calibration. However, the thermocouples were observed to get disturbed at the real size DC GIL arrangement, when a high DC current through the inner conductor was flowing. It is assumed that these disturbances result from the DC current source [10], which affects the temperature logger by EMI due to the conductive connection between the thermocouples and the inner conductor. This problem was overcome by collecting data only during cooling at different daytimes in the course of the on-site calibration. Using this method an online data logging was feasible, which made a large number of datapoints available for evaluation.

The DC GIL test arrangement was installed outdoor [2], which is why temperatures became weather dependent. The calibration was performed in spring, which offered ambient temperatures of the sensor in the range of $T_\mathrm{P,amb} = (10 \ldots 50)\,°\mathrm{C}$ due to sun radiation. The DC GIL was stressed with HL (high load – 3150 A), LL (low load – 1250 A) and ZL (zero load – 0 A). The LL operation was included, as in this condition the thermocouples were not disturbed by EMI yet. At the inner conductor temperatures in the range of $T = (10 \ldots 60)\,°\mathrm{C}$ were measured.

3.2 Results

As the best fit to interpolate the collected data, a linear polynomial approach was chosen. Equation (3) shows the used basic formula.

$$T_{\mathrm{calc}} = \mathrm{p}_{00} + \mathrm{p}_{10} T_{\mathrm{P}} + \mathrm{p}_{01} T_{\mathrm{P,amb}} \qquad (3)$$

$$\mathrm{p}_{00} = 0.1591, \mathrm{p}_{10} = 2.121, \mathrm{p}_{01} = -1.119$$

The coefficients p_{00}, p_{10} and p_{01} were determined based on the measurement results and are valid for the specific conditions of this test only. The most important temperature values for the long-term operation of a DC GIL are the maximum temperatures at HL operation. Therefore, these datapoints were weighted higher, so that their error is reduced. The resulting error between the conductor temperature T and the calculated temperature T_{calc} by use of equation (3) is shown in **Figure 6**.

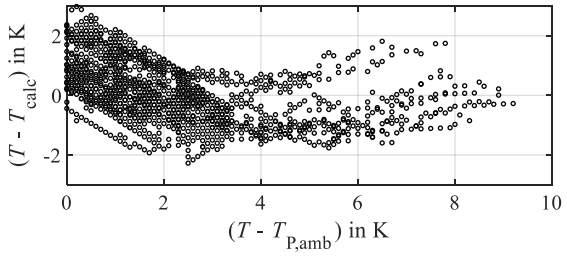

(a) Error over difference between conductor and ambient temperature

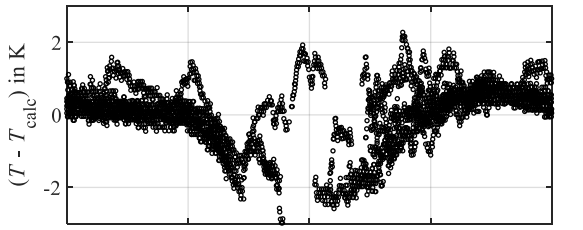

(b) Error over daytime

Figure 6 Measurement errors based on equation (3)

Figure 6 (a) shows a measurement error in the range of ±2.5 K, which tends to get larger for lower temperature differences $T - T_{\mathrm{P,amb}}$. This observation is in line to "finding 5" in **Table 1**. **Figure 6 (b)** shows that especially around 12 p.m. the error tends to increase. This is related to the strong sun radiation at this time, which also severely increases $T_{\mathrm{P,amb}}$. It is estimated that this observation is linked to the higher required re-adjusting time of the sensor in case of temperature change ("finding 4" in **Table 1**). In conclusion, the pyrometer sensor exhibits a higher error in the outdoor installation, compared to indoor installation. Overall, the approach according to equation (3) seems to be reasonable and delivers plausible data with acceptable errors. Potentially, the coefficients may depend on the sensor position, as the overall thermal setting would be different. It is thus recommended to check the calibration when pyrometer sensors are placed at different installation positions.

4 EMC Countermeasures

EMC countermeasures were applied to reduce the sensitivity to EMI of surrounding electrical devices and to avoid damages of the sensor electronics e.g. due to flashovers ("finding 2 and 3" in **Table 1**). Generally, all wire inputs and outputs were equipped with high frequency multiple wound ferrite beads. To further improve EMC, an additional electronic device was installed, placed directly at the pyrometer electronics (see 7 in **Figure 1**). The basic circuit to protect the pyrometer electronics is shown in **Figure 7**.

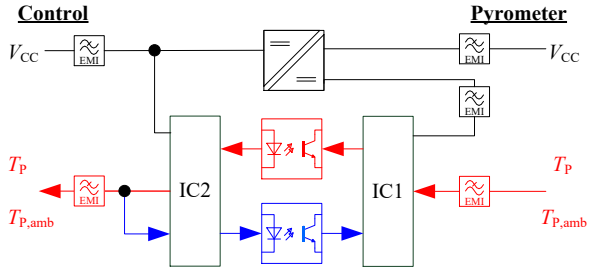

Figure 7 Basic electronic layout to protect the sensor electronics; ground connections not shown.

The additional device further protected each input/output such as T_{P} and $T_{\mathrm{P,amb}}$ and the power supply with EMI filters based on common mode chokes, surge arresters, capacitors and Zener diodes. Furthermore, the additional device was designed to fully isolate the electrical circuit of the pyrometer from the control cubical, to avoid EMI due to the required long connection wires. The electrical isolation of the power supply voltage V_{CC} was realized with isolated DC/DC converters. The isolation of the signals was realized with opto-couplers. The additional electronic module should add only a minimum additional error and temperature dependency to the signals T_{P} and $T_{\mathrm{P,amb}}$. For this purpose, two integrated circuits IC1 and IC2 were installed. Commercial ICs as well as microcontrollers may be used to fulfill the task. The ICs perform an analog/digital conversion of the signals and transmit them as frequency signals, which results in a low temperature dependency of the signal. To make sure that the signal at the control unit is as similar as possible to the pyrometer signal, a feedback loop (blue in **Figure 7**) is introduced, allowing IC1 to control its output.

The overall installation operated successfully during long-term operation, including events with high dU/dt and di/dt, which results in high EMI. During the on-site calibration it also showed a good suppression of EMI from the current source. Both would not have been possible without the additional unit.

5 Temperature measurements

Based on equation (3) the transient temperature stress during the long-term test can be calculated. The transient temperatures at the outdoor DC GIL installation strongly depend on weather and seasons. Besides the calculated

conductor temperature T_{calc}, the upper and lower enclosure temperatures $T_{encl,u}$, $T_{encl,l}$ were monitored as well (refer to **Figure 1**).

5.1 ZL Cycles

The pyrometer temperature measurement has a higher error during ZL cycles, as the ambient temperature of the sensor may get higher than the temperature of the inner conductor ("finding 5" in **Table 1**, **Figure 6 (a)**). This condition was mainly present between 6 a.m to 12 p.m, where the sun heated the overall outdoor assembly. Typical examples for summer and winter days are given in **Figure 8**.

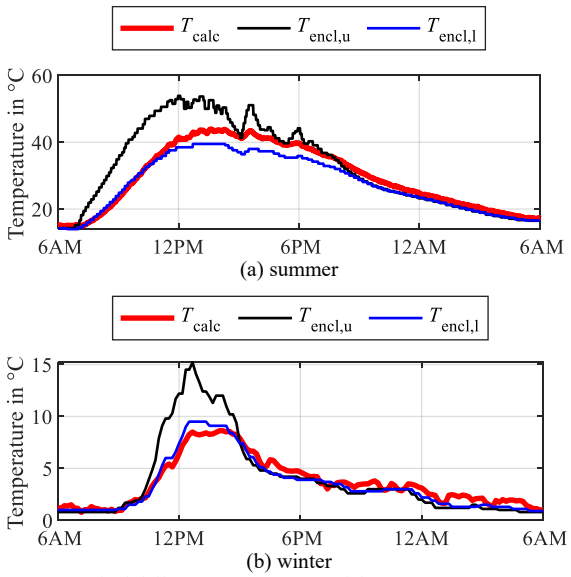

Figure 8 Typical daily ZL temperatures of the DC GIL arrangement

The sun has a large impact on the temperatures in both seasons. This especially becomes visible at the much higher upper enclosure temperature $T_{encl,u}$ than the lower $T_{encl,l}$. Steep increases and decreases of the temperatures may e.g. be related to clouds, which temporarily cover the sun. Under specific conditions as e.g. rain the conductor temperature may become temporarily higher than the enclosure temperature under ZL conditions, due to different thermal constants of the enclosure and the inner conductor temperature. Overall, both temperature courses seem to be plausible, as the inner conductor temperature T_{calc} is always approximately within the range of both enclosure temperatures $T_{encl,u}$ and $T_{encl,l}$.

5.2 HL Cycles

The calibration formula according to equation (3) is optimized for the higher HL temperatures. However, a larger error at 12 p.m. has to be expected (refer **Figure 6 (b)**). **Figure 9** shows examples of temperatures at the outdoor installed DC GIL on summer and winter days. During some summer days sun radiation was so strong that the temperature at the top of the enclosure was temporarily higher than at the inner conductor. In winter, this effect was less pronounced. The temperatures at the enclosure may significantly change during rainfall. This also affects the sensor ambient temperature $T_{P,amb}$. Since this temperature change appears fast, it is estimated that the transient pyrometer output has a larger error during rainfall as well ("finding 4" in **Table 1**). Again, both temperature courses in **Figure 9** seem to be plausible. The inner conductor temperature T_{calc} changes similar to the enclosure temperatures $T_{encl,u}$ and $T_{encl,l}$, but with a certain time delay, which seems to be plausible considering the larger thermal time constants, which were already observed in **Figure 8**.

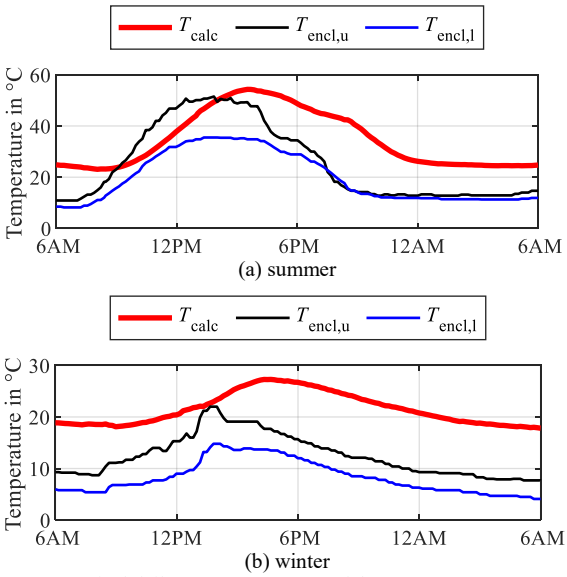

Figure 9 Typical daily HL temperatures of the DC GIL arrangement

6 Conclusions

Based on the gathered experience, a potential free temperature measurement with pyrometers in high-voltage GIS/GIL applications is feasible. Additional electronics are required to handle EMI, such as harmonics and impulses due to high-voltage flashovers. It is concluded that a laboratory calibration of the sensors based on a model arrangement is possible, considering the influencing factors given in the paper. The pyrometer measurement with the used sensor cannot be implemented by just adjusting the transmission and emission coefficients in the software, which indicates that the implemented algorithms inside the sensor electronics do not cover pressurized GIS and GIL systems with SF_6/N_2 gas atmosphere. Therefore, an equation was developed to calculate the temperature of the inner conductor based on the sensor output signals within certain error limits described in the paper. Temperature courses measured at HL and ZL in summer and winter show plausible data with the so calibrated sensor.

Future implementations of pyrometer measurements in gas insulated systems should consider the following aspects:

- If possible, pyrometers should be installed at the bottom of indoor installed gas insulated systems to minimize the influence of the ambient temperature.
- New pyrometers offer measurements in the range of (3...5) µm wavelength, where the transmission of SF_6 is $\tau \approx 1$. They are also described to react faster to

temperature changes. Such pyrometers might be better suited for gas insulated applications.

- The replacement of the sensitive sensor electronics in case of damage e.g. due to EMI is easier when placing the sensor outside the gas vessel and performing the measurement through a glass. This would also minimize the influence of the ambient temperature. However, the transmission of the glass will affect the pyrometer signal and has to be particularly considered.

Besides its usage in the regarded HVDC research project, pyrometer measurements in gas insulated systems are also of interest for other high-voltage applications. E.g. pyrometer measurement may become a tool for further research or future applications in DC as well as AC gas insulated systems.

7 Acknowledgment

The authors gratefully acknowledge the substantial support of this work by the IWB-EFRE-Program by the State of Hessen (Funding Code 20002558) and the German Federal Ministry of Economics and Technology (Funding Code 03ET7546).

8 Literature

[1] Cigré JWG D1.B3.57: “Dielectric testing of gas insulated HVDC systems”, CIGRE TB 842, 2021.

[2] M. Hallas, V. Hinrichsen, C. Neumann, M. Tenzer, B. Hausmann, D. Gross, T. Neidhart, M. Lerch, D. Wiesinger, “Cigré Prototype Installation Test for Gas-Insulated DC Systems – Testing a Gas-Insulated DC Transmission Line (DC-GIL) for ±550 kV and 5000 A under Real Service Conditions”, CIGRE D1-107, CIGRE Session 2020

[3] HOBO U12: „Deep Ocean Temp Logger“, Datasheet, Onset Computer Corporation, 470 MacArthur Boulevard, Bourne, MA 02532, USA

[4] Ekbert Hering, Gert Schönfelder: „Sensoren in Wissenschaft und Technik“, Vieweg+Teubner Verlag, 1st edition, pp.399-402, 2012

[5] Micro-Epsilon: “Grundlagen der berührungslosen Temperaturmessung”, online ressource, www.micro-epsilon.de, Micro-Epsilon Messtechnik GmbH & Co. Kg, Koenigbacher Str. 15, 94496 Ortenburg, Germany, accessed on 22. Jun. 2022

[6] NIST: “Sulfur hexafluoride”, online resource, https://webbook.nist.gov, National Institute of Standards and Technology, 100 Bureau Drive, Gaithersburg, MD 20899, USA - accessed on 22. Jun. 2022

[7] CTH-SF10-C3H: „thermoMETER CThot“, datasheet, Micro-Epsilon Messtechnik GmbH & Co. Kg, Koenigbacher Str. 15, 94496 Ortenburg, Germany

[8] Francis A. Kulacki: „Handbook of thermal Science and Engineering“, Springer Verlag, 1st edition, pp. 927, 2018

[9] Frank Bernhard: „Handbuch der Technischen Temperaturmesstechnik“, Springer Verlag, 2nd edition, pp. 1272, 2014

[10] M. Hallas, T. Wietoska, V. Hinrichsen: “Service Experience with a novel DC Current Injection Generator for HVDC Long-term Tests - 3150 A at 422 kV DC potential” In: 22nd International Symposium on High Voltage Engineering (ISH2021), Xi'an, PR China, 21.-25.11.2021

[11] P82919: “Pehapol-S 2K-Kunstoff-Lackfarbe – schwarz leitfähig” datasheet, Peter-Lacke GmbH, Herforder Strasse 80, 32120 Hiddenhausen, Germany